Research Journal of Pharmaceutical, Biological and Chemical Sciences

Synthesis and Characterization of Iron Oxide Nanoparticles and Applications in the Removal of Reactive Black 5H from Wastewater.

Ahmed M. Kamil, Mohammed A. Karam, Asim A. Balakit, and Falah H. Hussein[*].

College of Pharmacy, Babylon University, Hilla, Iraq .

ABSTRACT

This study investigated the preparation of iron oxide nanoparticles (Fe_2O_3). Fe_2O_3 nanoparticles were successfully synthesized by co-precipitation with sonication method. The prepared Fe_2O_3 was characterized by Fourier transform infrared spectrometry (FTIR), powder X-ray diffraction (XRD) and scanning electron microscopy (SEM). From XRD data, the product is hematite Fe_2O_3 and the crystal size is 49 nm. From the SEM photomicrographs, the particle size is 55 nm which is good agree with XRD results and indicate that the product has uniform spherical particles. The Fe_2O_3 nanoparticles were used to remove Reactive Black 5H (RB5H) from aqueous solution. The effects of contact time, Fe_2O_3 dosage and dye concentration on adsorption of RB5H dye by Fe_2O_3 were investigated. The equilibrium adsorption data was analyzed using three common adsorption models: Langmuir, Freundlich and Temkin. The adsorption study was analyzed kinetically, and the results revealed that the adsorption followed pseudo-second order kinetics with good correlation coefficients.
Keywords: Hematite, co-precipitation**,** RB5H**,** Adsorption.

*Corresponding author

INTRODUCTION

Recently, nanostructured materials have received significant interests because of their unique optical, electronic, magnetic and physicochemical properties that diverge greatly from their bulk materials. The nowadays tremendous amount of interest has been generated in the study of metal oxide materials because they lead to grow a new generation of sensors, photocatalysis, electrocatalysis, electronic, magnetic and adsorption applications [1-3].

Dyes have long been used in different types of industries such as dyeing, textiles, paper, plastics, leather and cosmetics [4]. Color stuff discharged from these industries poses hazards and has an environmental impact [5]. The presences of dyes in water are causing problems, such as, reducing oxygen levels in water; interfering with penetration of sunlight into waters; retarding photosynthesis and interfering with gas solubility in water bodies [6]. Dyes pollution is one of the most environmental problems; many methods have been used for removal of dyes from wastewater such as adsorption [7]. The adsorption technique proved to be an effective and attractive process for removing dyes from aqueous solutions in term of initial cost, ease of operation, insensitivity to toxic substance, high efficiency, easy recovery and simplicity of design [8, 9]. Different types of adsorbents have been used in the removal of dyes, including activated carbon [10, 11], carbon nanotubes [12–14], and metal oxides [15]. Among these adsorbents, iron nanomaterials have good properties, such as larger surface area, diminished consumption of chemicals and without secondary pollutant. Also, in recent years magnetic iron oxide nanomaterials was used to treat cancer by generation significant heat to cook tumor [16]. Iron oxide exists in a number of different phases such as hematite (α-Fe_2O_3), magnetite (Fe_3O_4), akaganeite (β-Fe_2O_3) and maghemite (γ-Fe_2O_3) [17].

There are different chemical methods to prepare iron oxide nanoparticles, including gas phase methods (reduction, hydrolysis, disproportionation, oxidation, or other reactions to precipitate solid products from the gas phase), that depend on thermal decomposition [18], liquid phase methods, two-phase methods, sol–gel methods, high pressure hydrothermal methods [19] and co-precipitation [20–22]. Among these various chemical methods, The co-precipitation method is the most effective technique for preparing aqueous dispersions of iron oxide nanoparticles because good homogeneity, low cost, high purity of product and not requiring organic solvents and heat treatment.

In this article, iron oxide nanoparticles were prepared using a co - precipitation method. The sample was dried and calcined at 650 °C for one hour. The prepared sample was characterized by X-ray diffraction (XRD), Fourier transform infrared spectroscopy (FTIR). The main objective of this research was to evaluate the adsorption ability of the prepared iron oxide for the removal of Reactive Black 5H (RB5H). The effects of contact time, iron oxide dosage and initial dye concentration on the adsorption capacity were studied.

EXPERIMENTAL

Chemicals

Iron sulfate ($FeSO_4.7H_2O$) and sodium hydroxide (NaOH) were purchased from Merck. $FeSO_4.7H_2O$ and NaOH were used without further purification. RB5H was purchased from Hilla textile factory. Double distilled water was used to prepare the precursor solution.

Preparation of Iron Oxide Nanoparticles

$FeSO_4.7H_2O$ was dissolved in 100 mL of 5% sulfuric acid solution to form an iron precursor solution with a 0.5 M concentration. The solution was bubbled with Argon gas to prevent unwanted oxidation. The NaOH solution (20%) was dropped to this solution with vigorous sonication at 80 °C until pH 10. The reaction was continued at that temperature for 30 min before the reactor was removed by heating and sanitation, and then the gray solution was stirred for 60 min. The brown precipitate was then collected by filtration and washed with distilled water to natural pH. Finally, the washed precipitate was dried at 90 °C and calcined at 600 °C for one hour.

Characterization Methods

X-ray diffraction (XRD) spectra were collected on a Phillips PW 1800 with a positional sensitive detector using monochromatic Cu Kα radiation.

XRD data were employed to calculate the average crystallite sizes (D) by Scherrer's formula in the following equation [23]:

$$D = \frac{k\lambda}{\beta cos\theta}$$

1

where: D is the average crystal size, k = 0.94 is the constant crystal lattice, λ = 0.154 nm is the X-ray wavelength of Cu Kα, β is the full width of the peak measured at half maximum intensity and ϑ is the Bragg's angle of the peak.

IR spectra were recorded on a Bruker tensor 27 FTIR spectrometer with RTDLATGS detector. The analyzed sample was measured within a range of (4000-500) cm^{-1} on a pallet with a KBr dose at room temperature.

Scanning electron microscopy (SEM) measurements were carried out on a JEOL – JSM-6700F Japan instrument, using a secondary electron detector (SE) at an accelerating voltage of 26 kV.

Adsorption Kinetic Experiments

For kinetic studies, solutions of 30, 40, 50 and 60 mg/L RB5H, as the initial concentration, were treated with 1 g of prepared iron oxide at a constant temperature of 298.15 K. The mixtures were then subjected to agitation using a shaker (Gemmy orbit, van 480 Gemmy Industrial Corp-Taiwan). In all cases, the working pH of solution was not controlled. Mixtures were taken from the shaker at appropriate time intervals (10, 20, 30, 40, 50, 60 min). The suspensions were filtered using a centrifuge and the filtrates were analyzed for residual RB5H concentration by UV-visible spectrophotometer (PG instruments Ltd- Japan) at 567 nm.
The amount of RB5H uptake by the prepared iron oxide in each flask was calculated using the mass balance equation:

$$q_t = \frac{(C_0 - C_t) \times V}{W}$$

2

where q_t is the amount of RB5H adsorbed by the prepared iron oxide at time (t), C_o and C_t are the initial and dye concentrations at time (t), respectively, V is the volume of solution (L), and W is the adsorbent weight (g). The dye percent removal (%) was calculated using the following equation:

$$Removal\ \% = \frac{C_0 - C_t}{C_0} \times 100$$

3

RESULTS AND DISCUSSION

Characterization of the Prepared Iron Oxide

FTIR studies were performed to ascertain the metal–oxygen bonding. The FTIR spectrum of as synthesized Fe_2O_3 sample is shown in Figure 1. The Fe_2O_3 shows the absorption in the regions 527.44, 1037.13, 1637.52 and 3448.59 cm^{-1}. The peak at 527.44 cm^{-1} refers to the metal–oxygen vibrational modes [24]. The peak at 1037 cm^{-1} it can be inferred that this sample contains a significant amount of adsorbed sulphate groups [25]. The peaks at 1637.13 cm^{-1} and 3448.59 cm^{-1} are due to the OH bending of water and the hydroxyl group ($^-$OH), respectively [26]. The peak at 2.362 cm^{-1} due to the presence of atmospheric CO_2 [27].

The XRD patterns of the prepared Fe_2O_3 nanoparticles were illustrated in Figure 2. The peaks appeared at 2θ range of 24.2°,33.2°, 35.7°, 40.9°, 49.5°, 54.1° and 57.6° can be attributed to the 012, 104, 110,

113, 024, 116 and 018 diffraction planes of hematite α-Fe_2O_3 [28]. No impurity peak indicates that the product is pure. According to the Scherrer's equation, the average crystallite size was calculated to be about 49 nm. Average particle size and morphology of nanoparticles were studied using a JEOL – JSM-6700F scanning electron microscope. The SEM images are shown in Figures 3. The prepared nanoparticles fabricated via co-precipitation with sonication process have very homogenous morphologies with spherical shapes, regular dispersion and are well crystallize in nature. The average particle size of the nanoparticles is 55 nm which is in agreement with XRD results. These results suggest that the nanoparticles are a single crystal [29]. The agglomeration was occurred in the iron oxide nanopowders. The agglomeration is due to van der Waals force between particles and may be to humidity.
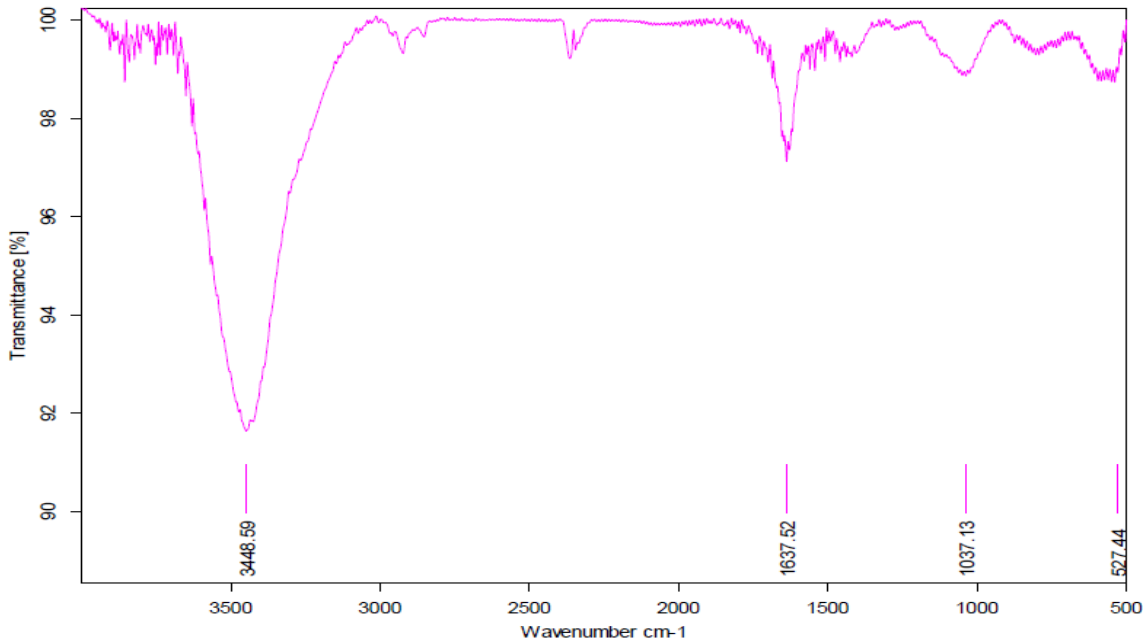

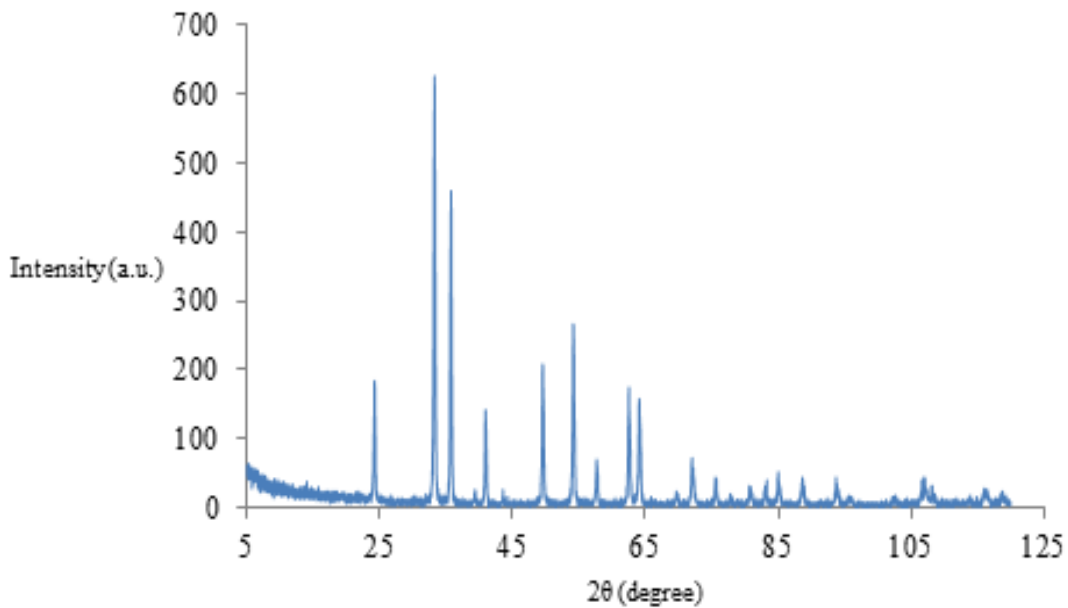**Figure 1: FTIR spectrum of the prepared Fe_2O_3.**
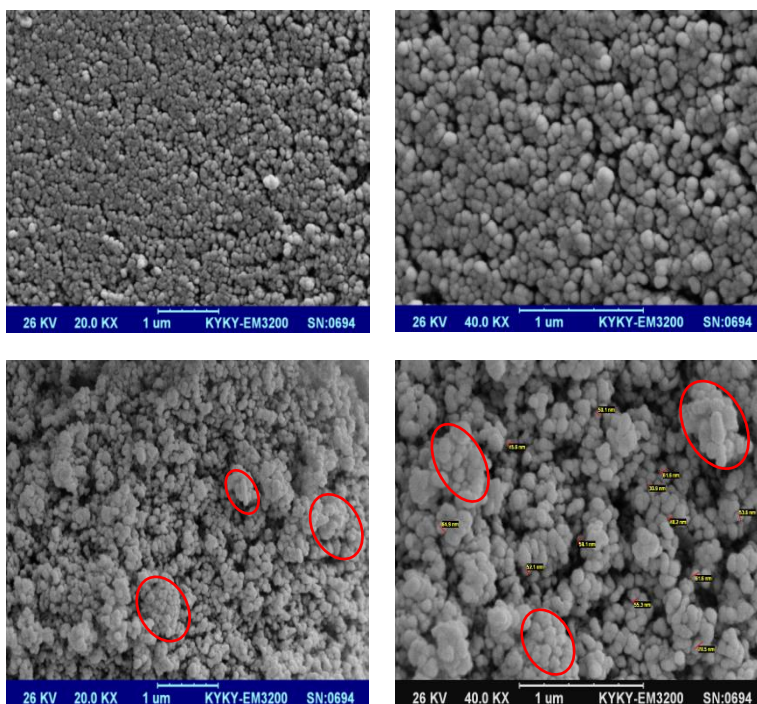

Figure 2: XRD of the prepared Fe_2O_3.

Figure 3: SEM images of the prepared Fe_2O_3.

Effect of Contact Time

The effect of contact time on the adsorption capacity of RB5H onto the prepared iron oxide is shown in Figure 4, When the initial RB5H concentration has increased from 30 to 60 mg/L the amount of RB5H adsorbed onto the prepared iron oxide, at 60 min contact time, 1 g adsorbent dose and the constant temperature 298.15 K, increased from 2.9 to 5.7 mg g^{-1}. The increase of loading capacity of the prepared iron oxide with increasing initial RB5H concentration may be due to higher interaction between RB5H and adsorbent [30, 31]. These results show that rapid increase in the adsorbed amount of RB5H is achieved during the first 10 minutes.
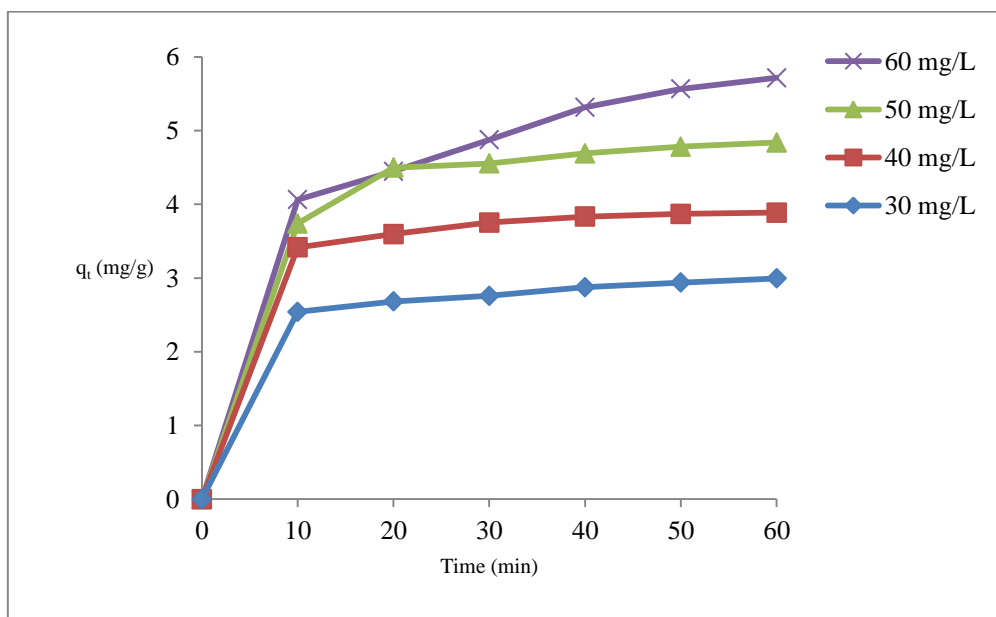

Figure 4: Effect of contact time on the adsorption of RB5H dye by the prepared iron oxide.

Effect of the Prepared Iron Oxide Dosage

To determine the effect of adsorbent dosage on the adsorption of RB5H, a series of adsorption experiments were carried out with different adsorbent mass at an initial dye concentration of 50 mg/L. Figure 5 shows the effect of adsorbent dose on the removal of RB5H. The increasing of adsorbent dosage from 0.1 to 1.5 g, the percentage of dye adsorbed increased from 18.2 to 99.5% after 60 min of adsorption time. This result was expected that as the number of available adsorption sites increases by increasing the adsorbent amount [32, 33].
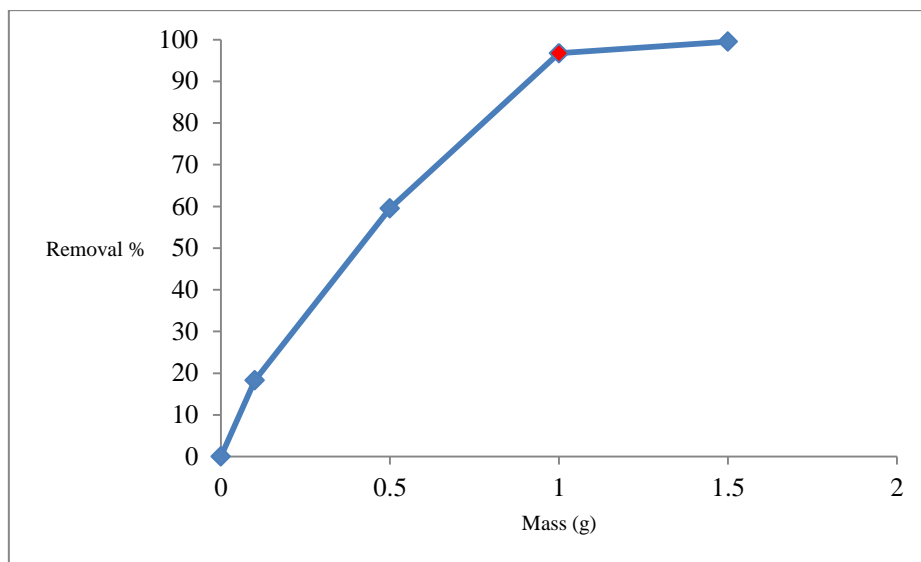

Figure 5: Effect of the prepared iron oxide dose on the removal percentage of RB5H.

Effect of Initial Concentration of RB5h Dye

Different concentrations of RB5H 30, 40, 50 and 60 mg/L, were selected to study the effect of initial concentration of dye onto the prepared iron oxide. The amounts of dye adsorbed adsorbent dosage 1 g and 298.15 K are given in Figure 6. With increasing initial concentration of RB5H from 30 to 60 mg/L, the removal percent of dye molecules decreases from 99.7 to 95.2% after 60 min of adsorption time. These results agree with adsorption of orange II dye in aqueous solution onto surfactant-coated zeolite: characterization, kinetic and thermodynamic studies [34].
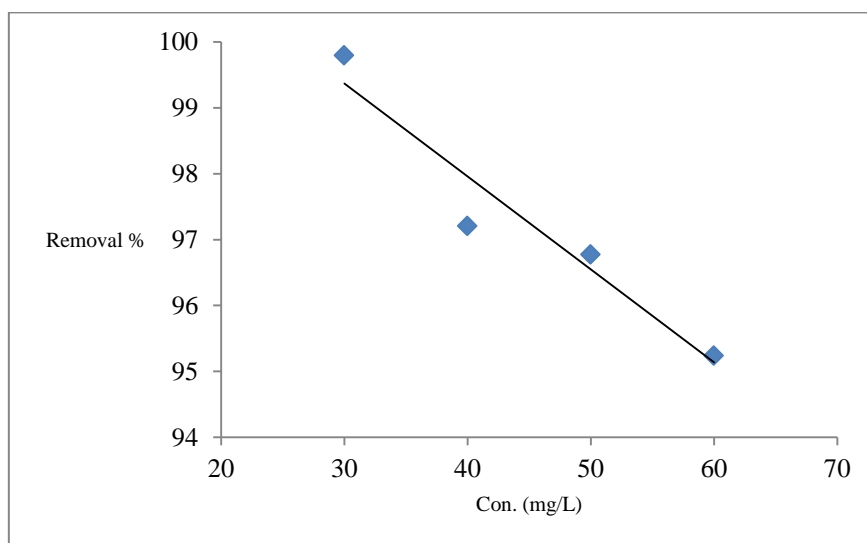

Figure 6: Effect of initial concentrations on the adsorption percentage of RB5H on the prepared iron oxide.

Adsorption Isotherm

The isotherm provides a relationship between the concentration of dye in solution and the amount of dye adsorbed on the solid phase when both phases are in equilibrium. The equilibrium of experimental data for adsorbed RB5H on the prepared iron oxide was studied by using the Langmuir, Freundlich and Temkin isotherm models.

Langmuir Isotherm

The Langmuir adsorption isotherm assumes that adsorption takes place at specific homogeneous sites within the adsorbent and has found successful application in many sorption processes of monolayer adsorption [35]. Figure 7 shows the Langmuir isotherm for adsorption RB5H on the prepared iron oxide. The following equation is the Langmuir isotherm:

$$\frac{C_e}{q_e} = \frac{1}{q_m K_L} + \frac{C_e}{q_m} \qquad\qquad 4$$

where q_m is the maximum amount of the RB5H adsorbed per unit mass of MWCNTs, and K_L is the Langmuir constant related to the rate of adsorption.
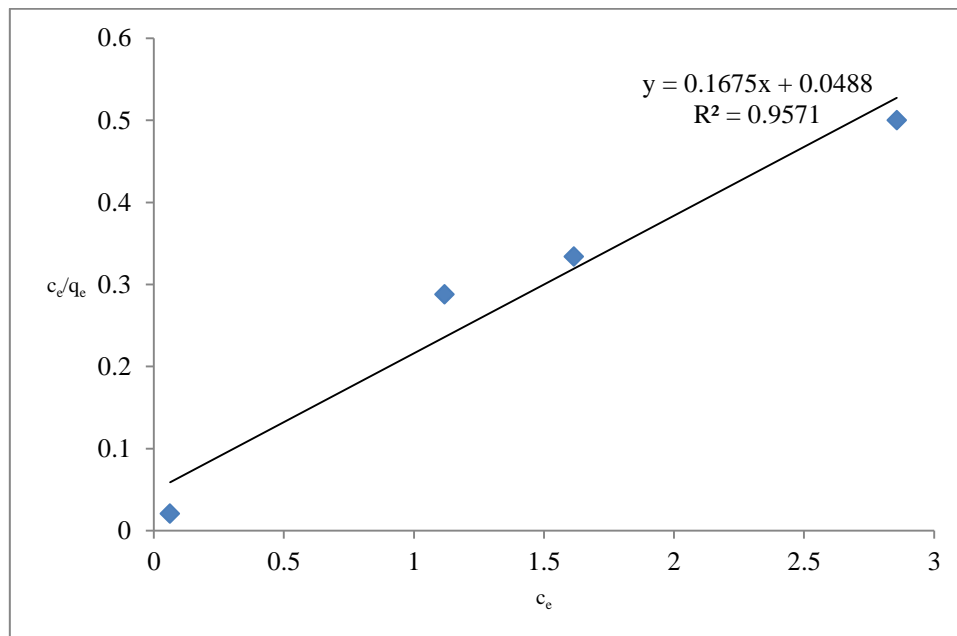

Figure 7: Langmuir isotherm for RB5H adsorption onto the prepared iron oxide.

For the Langmuir equation, the favorable nature of adsorption can be expressed in terms of the dimensionless separation factor of equilibrium parameter (R_L) [36], which is defined by:

$$R_L = \frac{1}{1 + K_L C_o} \qquad\qquad 5$$

where R_L is the dimensionless equilibrium parameter. The values of R_L indicate the type of isotherm to be irreversible ($R_L = 0$), favorable ($0 < R_L < 1$), linear ($R_L = 1$) or unfavorable ($R_L > 1$) [37]. The values of the dimensionless separation factor are given in Table 1.

Table 1: The dimensionless separation factor for the adsorption of RB5H on the prepared iron oxide.

Con./ppm	R_L
30	0.82
40	0.20
50	0.15
60	0.09

Freundlich Isotherm

The Freundlich isotherm is an empirical equation employed to describe heterogeneous systems [38]. The Freundlich model is based on the distribution of an adsorbate between an adsorbent and the aqueous phases at equilibrium [39]. Figure 8 shows the Freundlich isotherm for adsorption RB5H on the prepared iron oxide. The basic Freundlich equation is:

$$log(q_e) = logK_F + \frac{1}{n}log\,C_e \qquad\qquad 6$$

where: K_F and n are Freundlich constants, which allows a measure of adsorption capacity and adsorption intensity, respectively.
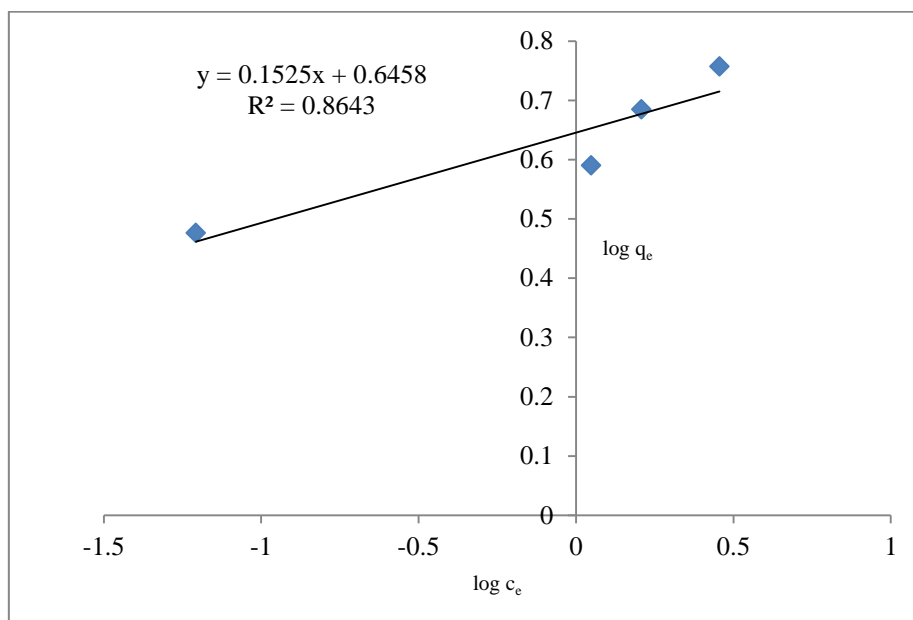

$$y = 0.1525x + 0.6458$$
$$R^2 = 0.8643$$

Figure 8: Freundlich isotherm for RB5H adsorption on the prepared iron oxide.

Temkin Isotherm

This isotherm takes into account the indirect adsorbate-adsorbent interactions on adsorption isotherms, and suggests that because of these interactions the heat of the adsorption of all the molecules in the layer would decrease linearly with coverage [40]. Figure 9 shows the Temkin isotherm for adsorption RB5H on the prepared iron oxide. The Temkin isotherm has been used in the form given below:

$$q_e = B_1 lnC_e + B_1\,ln \qquad\qquad 7$$

where K_T and B_1 are the Temkin constants (K_T is the equilibrium binding constant (L/g) and B_1 is related to the heat of adsorption). The values of the isotherm parameters are given in Table 2.
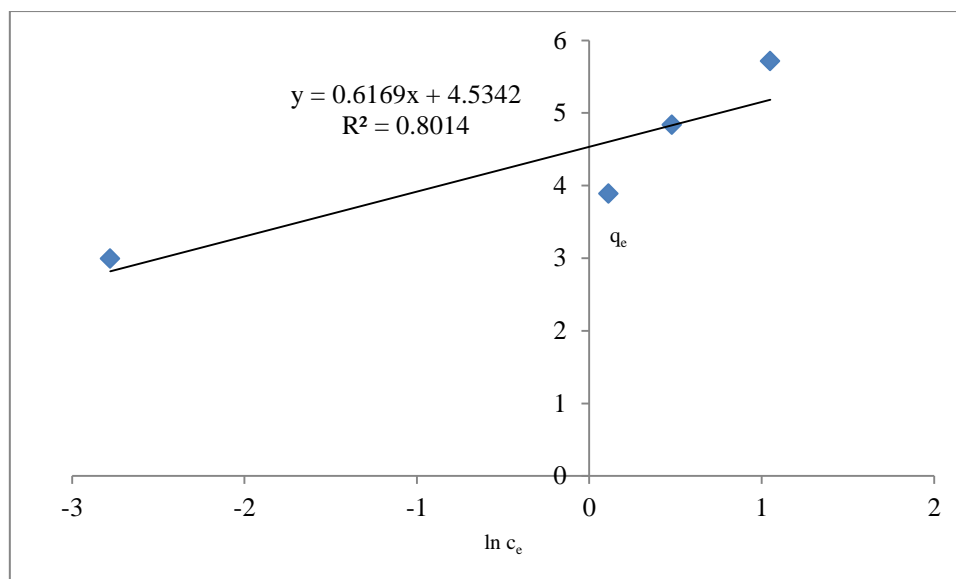
y = 0.6169x + 4.5342
R² = 0.8014

Figure 9: Temkin isotherm for RB5H adsorption onto the prepared iron oxide.

Table 2: The adsorption constants of the Langmuir, Freundlich and Temkin isotherms.

Isotherms	Parameters	Values
Langmuir	Q_m	5.9
	K_L	3.4
	R^2	0.9571
Freundlich	K_F	1.9
	n	6.5
	R^2	0.8643
Temkin	B_1	0.6169
	K_T	1556
	R^2	0.8014

Adsorption Kinetics

Three kinetic models: Pseudo-first order, pseudo-second order and Intra particle diffusion kinetic models were used to fit experimental data to examine the adsorption kinetics. Equations 8, 9 and 10 represent the linear forms of the pseudo-first order, pseudo-second order models and Intra particle diffusion kinetic model respectively.

$$ln(q_t - q_e) = ln(q_e) - k_1 t \qquad\qquad 8$$
$$\frac{t}{q_t} = \frac{1}{k_2 q_e^2} + \frac{t}{q_e} \qquad\qquad 9$$
$$q_t = k_3 t^{1/2} + C \qquad\qquad 10$$

The straight-line plots of $ln(q_e-q_t)$ versus t for the pseudo-first order reaction (Figure 10), t/q_t versus t for the pseudo-second order reaction (Figure 11) and q_t versus $t_{1/2}$ for the Intra particle diffusion reaction (Figure 12) for adsorption of RB5H onto the prepared iron oxide. The values of the kinetic parameters and correlation coefficient were calculated from these plots are given in Table 3. The pseudo-second order model best represents this experimental data.
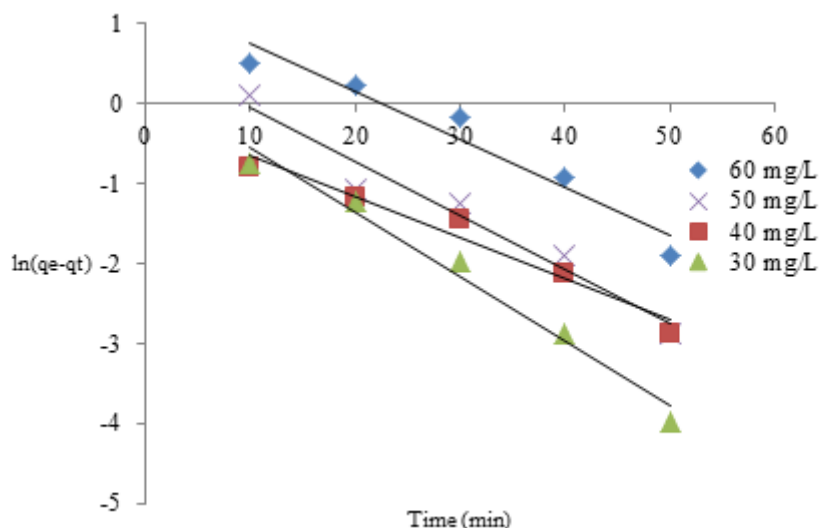
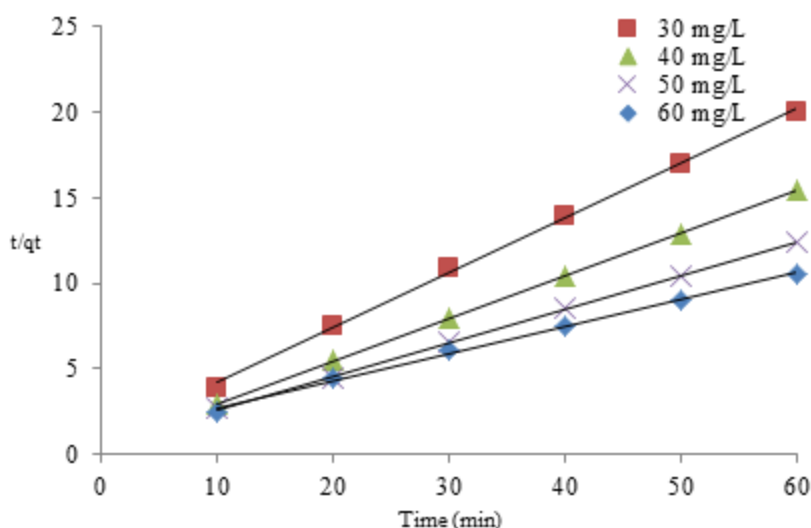**Figure 10: Pseudo-first order kinetic model for the adsorption of RB5H on the prepared iron oxide.**

Figure 11: Pseudo-second order kinetic model for the adsorption of RB5H on the prepared iron oxide.

Table 3: The adsorption parameters for adsorption RB5H on the prepared iron oxide.

| Con./ppm	Pseudo first order model			
	$q_{e,exp}$ (mg/g)	$q_{e,cal}$ (mg/g)	K_1 (min^{-1})	R^2
30	2.9	0.8	0.0515	0.9605
40	3.8	1.3	0.0812	0.9799
50	4.8	1.8	0.0679	0.9561
60	5.7	3.8	0.0597	0.9408
Con./ppm	Pseudo second order model			
	$q_{e,exp}$ (mg/g)	$q_{e,cal}$ (mg/g)	K_2 (g/mg min)	R^2
30	2.9	3.1	0.3268	0.999
40	3.8	4.0	0.4873	0.9999
50	4.8	5.1	0.2984	0.9996
60	5.7	6.3	0.1327	0.9954
Con./ppm	Intra particle diffusion model			
	$q_{e,exp}$ (mg/g)	c (mg/g)	K_3 (mg/g min$^{1/2}$)	R^2
30	2.9	2.2	0.1000	0.9952
40	3.8	3.1	0.1062	0.9493
50	4.8	3.2	0.2160	0.8313
60	5.7	2.8	0.3822	0.9899
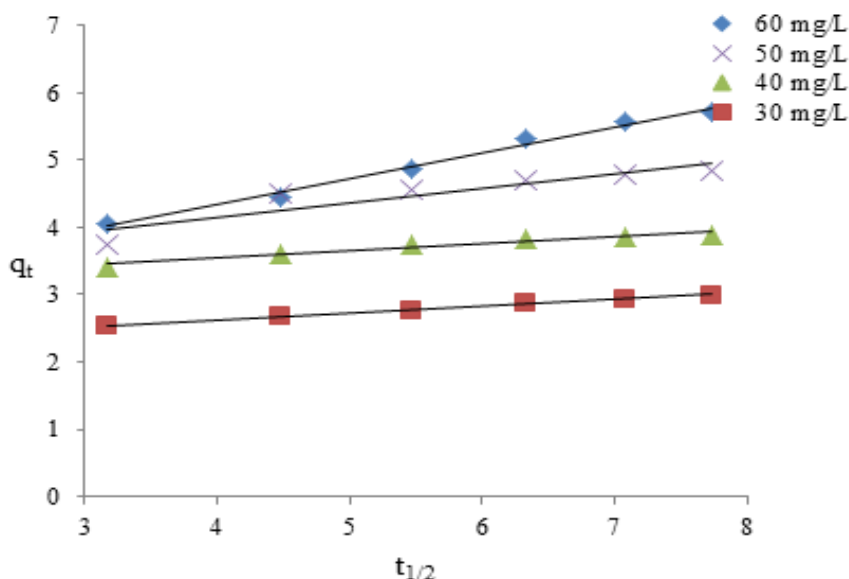
Figure 12: Intra particle diffusion model for the adsorption of RB5H on the prepared iron oxide.

CONCLUSIONS

Iron oxide adsorbent was prepared using a co-precipitation method. The FTIR spectroscopy shown several vibration bands at various wave numbers confirm the formation of Fe_2O_3 nanoparticles. The XRD patterns indicated that the prepared iron oxide nanoparticles were hematite with average crystallite size equal to 49 nm. The SEM analysis illustrates that the average particles size around 55 nm, and particle shape was a sphere. The SEM analysis refers the monocrystalline structure of Fe_2O_3 nanoparticles. The prepared Fe_2O_3 nanoparticles were used for the removal of RB5H from aqueous solution. 1 g is the optimum dosage of Fe_2O_3 to adsorb 50 mg/L of RB5H. The adsorption capacity of the RB5H on Fe_2O_3 nanoparticle increased with the increasing of initial concentration of RB5H. The optimum contact time was 10 min. The adsorption kinetics was fitted by a pseudo-second order kinetic model. The adsorption of the RB5H on Fe_2O_3 nanoparticle has been described by the Langmuir, Freundlich and Temkin adsorption isotherm models. R_L values indicate favorable adsorption.

REFERENCES

[1]   Zhang X, Janekhe SA, Perlstein J. Chem. Mater 1996; 8(8): 1571-1574.
[2]   Fendler JH. Chem Mater 1996; 8(8): 1616-1624.
[3]   Madhusudhana N, Yogendra K, Mahadevan KM. Res. J. Chem. Sci. 2012; 2(5): 72-77.
[4]   Hussein FH, Halbus AF. International Journal of Photoenergy 2012; 2012: 1-9.
[5]   Crini G. Bioresour Technol 2006; 97(9): 1061-1085.
[6]   Garg VK, Amita M, Kumar R, Gupta R. Dyes Pigments 2004; 63(3): 243-250.
[7]   Kamil AM, Abdalrazak FH, Halbus AF, Hussein FH. Environmental Analytical Chemistry 2014; 1(1): 1-6.
[8]   Mitchell M, Ernst WR, Rasmussen ET, Bagherzadeh P, Lightsey GR. Bull Environ Contam Toxicol 1978; 19(1): 307-311.
[9]   Garg VK, Gupta R, Bala YA, Kumar R. Bioresour Technol 2003; 89(2): 121-124.
[10]   Kang KC, Kim SS, Choi JW, Kwon SH. Journal of Industrial and Engineering Chemistry 2008; 14(1): 131–135.
[11]   Jusoh A, Shiung LS, Ali N, Noor MJMM. Desalination 2007; 206(1–3): 9–16.
[12]   Li YH, Liu FQ, Xia B, Du QJ, Zhang P, Wang DC, Wang ZH, Xia YZ. Journal of HazardousMaterials 2010; 177(1-3): 876–880.
[13]   Kandah MI, Meunier JL. Journal of Hazardous Materials 2007; 146(1-2): 283–288.
[14]   Li YH, Di Z, Ding J, Wu D, Luan Z, Zhu Y. Water Research 2005; 39(4): 605–609.
[15]   Ai Z, Cheng Y, Zhang L, Qiu J. Environmental Science and Technology 2008; 42(18): 6955–6960.
[16]   NDong C, Tate AJ, Kett WC, Batra J, Demidenko E, Lewis LD, Hoopes P.J, Gerngross TU, Griswold KE. PLOS ONE 2015; 10(2): 1-18.

[17]   Mohapatra M, Anand S. International Journal of Engineering, Science and Technology 2010; 2(8):127-146.
[18]   Pierson HO. Handbook of Chemical Vapor Deposition: Principles, Technology, and Applications. William Andrew Inc, 1999; pp.174.
[19]   Teja AS, Koh PY. Prog. Cryst. Growth Charact Mater. 2009; 55(1-2): 22–45.
[20]   Lee SJ, Jeong JR, Shin SC, Kim JC, Kim JD. J. Magn. Magn. Mater. 2004; 282: 147- 150.
[21]   Darezereshki E. Mater. Lett. 2010; 64(13): 1471–1472.
[22]   Layek S, Pandey A, Pandey A, Verma HC. Int. J. Eng. Sci. Technol. 2010; 2(8): 33–39.
[23]   Scherrer P. Mathematisch- Physikalische Klasse 1918; 2: 98–100.
[24]   Jarlbring M, Gunneriusson L, Hussmann B, Forsling W. J. Colloid Interf. Sci. 2005; 285(1): 212–217.
[25]   Goticand M, Music S. Journal of Molecular Structure 2007; 834-836: 445–453.
[26]   Walter D. Thermochim. Acta 2006; 445(2): 195–199.
[27]   Chakrabarti S, Ganguli D, Chaudhuri S. J. Physica. E Low-dimensional Systems and Nanostructures 2004; 24(3-4): 333-342.
[28]   Farahmandjou M, Soflaee F. Phys. Chem. Res. 2015; 3(3): 191-196.
[29]   Nedkov I, Merodiiska T, Milenova L, Koutzarova T, J. Magn. Magn. Mater. 2000; 211(1-3): 296-300.
[30]   Aroua MK, Leong SP, Teo LY, Yin CY, Daud WM. Bioresour Technol 2008; 99(13): 5786-5792.
[31]   Lafta AJ, Halbus AF, Baqir SJ, Hussein FH. Research Journal of Pharmaceutical, Biological and Chemical Sciences 2015; 6(6): 1115-1123.
[32]   Lafta AJ, Halbus AF., Athab ZH, Kamil AM, Hussein AS, Qhat AF, Hussein FH. Asian Journal of Chemistry 2014; 26: S119-S123.
[33]   Boughachiche A, Bouhouf L, Boukhalfa C. Research Journal of Pharmaceutical, Biological and Chemical Sciences 2015; 6(6): 945-952.
[34]   Jin X, Yu B, Chen Z, Arocena JM., Thring RW. Journal of Colloid and Interface Science 2014; 435: 15-20.
[35]   Langmuir I. The Journal of the American Chemical Society 1918; 40: 1361-1403.
[36]   Webi TW, Chakravorti RK. AI Ch E Journal 1974; 20(2): 228-238.
[37]   Hamdaoui O. J Hazard Mater 2006; 135(1-3): 264-273.
[38]   Wang S, Boyjoo Y, Choueib A. Chemosphere 2005; 60(10): 1401-1407.
[39]   Freundlich H. Journal of Physical Chemistry 1985; 57: 387-470.
[40]   Temkin M, Pyzhev V. J Phys Chem 1940; 13(7): 851-867.